Testing the Maximum Entropy Production approach for estimating evapotranspiration from closed canopy shrubland in a low-energy humid environment

Journal:	*Hydrological Processes*
Manuscript ID	HYP-17-0444.R2
Wiley - Manuscript type:	Scientific Briefing
Date Submitted by the Author:	n/a

Complete List of Authors:	Wang, Hailong; University of Aberdeen, School of Geosciences Tetzlaff, Doerthe; University of Aberdeen, Northern Rivers Institute, School of Geosciences Soulsby, Chris; University of Aberdeen, School of Geosciences

Keywords:	evapotranspiration, water balance, interception, climate change, northern uplands, maximum entropy production

Testing the Maximum Entropy Production approach for estimating evapotranspiration from closed canopy shrubland in a low-energy humid environment

Hailong Wang*, Doerthe Tetzlaff, Chris Soulsby

Northern Rivers Institute, School of Geosciences, University of Aberdeen, AB24 3UE, United Kingdom

*corresponding to hailong.wang@abdn.ac.uk; whl84@hotmail.com; +44 1224 272342

Emails of co-authors:

Doerthe Tetzlaff: d.tetzlaff@abdn.ac.uk

Chris Soulsby: c.soulsby@abdn.ac.uk

Abstract: Quantifying and partitioning evapotranspiration (*ET*) into evaporation (*E*) and transpiration (*T*) is challenging but important for interpreting vegetation effects on the water balance. We applied a model based on the theory of maximum entropy production (MEP) to estimate *ET* for shrubs for the first time in a low-energy humid headwater catchment in the Scottish Highlands. In total, 53% of rainfall over the growing season was returned to the atmosphere through *ET* (59±2% as transpiration), with 22% of rainfall ascribed to interception loss and understory *ET*. The remainder of rainfall percolated below the rooting zone. The MEP model showed good capability for total *ET* estimation, in addition to providing a first approximation for distinguishing *E* and *T* in such ecosystems. This study shows that this simple and low-cost approach has potential for local to regional *ET* estimation with availability of high-resolution hydroclimatic data. Limitations of the approach are also discussed.

Key words: evapotranspiration; water balance; interception; climate change; northern uplands; maximum entropy production

1. Introduction

Northern high latitude ecosystems are experiencing amplified climate warming (Serreze and Barry, 2011; IPCC, 2014) which has led to changes in the composition, density and distribution of vegetation communities in recent decades (Elmendorf *et al.*, 2012); for example, a northward advance of the tree-line replacing tundra shrubs (Serreze and Barry, 2011; Yu *et al.*, 2014). Future drying and warming in growing seasons (Lindner *et al.*, 2008) may lead to a reduction in subsurface water storage and streamflow due to increasing evapotranspiration (*ET*). In water-limited areas, annual *ET* can account for over 90% of precipitation (Wilcox *et al.*, 2006). Whilst the evaporation (*E*) component of *ET* is essentially a water loss, transpiration (*T*) is related to biomass production (Kool *et al.*, 2014), though constrained by both plant physiological and environmental factors such that stomata can respond to stress imposed by high vapor pressure deficit or low root-zone soil water content (Wang *et al.*, 2014). The proportion of *E* dominates over bare soil and sparsely vegetated surfaces (Lu *et al.*, 2017); while *T* is usually greater over densely vegetated areas and in energy limited regions (Miralles *et al.*, 2011; Schlesinger and Jasechko, 2014). Estimating and partitioning *ET* is crucial to provide evidence for sustainable water management that targets high water use efficiency, especially in a time of marked environmental change.

Whilst the physics are understood (Brutsaert, 1982; Allen *et al.*, 1996), we still have difficulties in estimating actual *ET* in the landscape. Kool *et al*., (2014) summarized *ET* partitioning methods ranging from field measurements to remote sensing algorithms. Eddy covariance and Bowen ratio techniques commonly provide total over-canopy *ET* measurements mostly in flat terrain and for homogeneous vegetation covers (Baldocchi *et al.*, 2001). Other methods such as sap flow measurements (Granier, 1987) and mass balance of stable isotopes (Sutanto *et al.*, 2012) can provide separate estimates of *E* and *T*. However, such field techniques are often difficult to extrapolate to a broader scale, and have high costs to setup and maintain instruments, particularly in remote areas with complex topography and heterogeneous vegetation cover (Caylor *et al.*, 2006). Surface energy balance-based remote sensing algorithms (e.g., Shuttleworth and Wallace, 1985) can provide long-term *ET* estimates for large spatial areas, but usually are not able to provide *ET* at high spatiotemporal resolutions due to low satellite orbiting frequency and high cloud cover (Shwetha and Kumar, 2015) in some high latitude regions. Hydrological models can help understand interlinkages between different water balance components, though such models usually require large input datasets (Chen *et al.*, 2007) to calibrate parameters (often unidentifiable) commonly against streamflow (van Huijgevoort *et al.*, 2016). *ET* parameterization in such models is either overly simple (e.g., van Huijgevoort *et al.*, 2016) or extremely complex (e.g., Noilhan and Planton, 1989).

Recently, a novel and simple approach for *ET* estimation was proposed based on the theory of maximum entropy production (MEP), and tested over dry land surfaces (Wang and Bras, 2009, 2011). The model only requires net radiation (*Rn*), temperature and specific humidity measured at soil and canopy surfaces for *E* and *T* estimation respectively. The model differs to conventional bulk transfer approaches in several ways (Bras, 2015): water and energy fluxes are estimated without using temperature and humidity gradients; wind speed and surface roughness are not needed to parameterize turbulent transport; and surface energy balance is always and automatically conserved. Notably, previous application of the MEP model was focused on either bare soil for evaporation or full vegetation cover for transpiration. Whilst total *ET* estimation using the MEP model over vegetated surfaces can substantially reduce measurement efforts, the approach has not yet been fully tested.

Here, we focus on a humid, low-energy heather (*Calluna vulgaris* and *Erica tetralix*) shrub ecosystems in NE Scotland (Tetzlaff *et al.*, 2015). Heather moorland is the third most extensive land cover in the UK (Stewart *et al.*, 2008), and the characteristics of its growth, development and ecology have been well documented (Gimingham, 1960; MacDonald *et al.*, 1995). However, the potential effects of the complex nature of heather canopy on water and energy exchange with atmosphere are not well investigated, and studies on water use and interception in heather-dominated areas are limited to several in the British uplands around 1980s and 1990s (Wallace *et al.*, 1982; Calder *et al.*, 1984; Miranda *et al.*, 1984; Calder, 1986; Dunn and Mackay, 1995;

Haria and Price, 2000). Though annual *ET* is usually modest compared to other water budget components in the Scottish Highlands (Soulsby *et al.*, 2015), its quantification is crucial for assessing the role of land use in water fluxes and stores (Calder, 1986; Ladekarl *et al.*, 2005). Therefore, in this study we applied the MEP model to test its capability for providing total *ET* estimation and partitioning in such an ecosystem. Subsequently, we quantified the water budgets to enhance our understanding of the vegetation effects on water partitioning in terms of *T, E* and deep percolation. We also discussed the strengths and weaknesses of the approach in this environmental setting.

2. Data and Methods

2.1. Study site and measurements

The Bruntland Burn (57.04ºN, 3.13ºW, Figure 1) in the Scottish Highlands represents a low-energy, high-humidity headwater catchment in northerly latitudes at the temperate/boreal transition (Tetzlaff *et al.*, 2014; Soulsby *et al.*, 2015). The catchment has an elevation of 250-500 m.a.s.l, with gentle slopes across most areas and only steep slopes in the upper areas. Annual precipitation (*P*) is over 1000 mm of which only <5% is snow. There are no distinct dry and wet seasons since *P* is fairly evenly distributed throughout the year, with a monthly average of 74±15 mm and a median of 68 mm over the last three decades. Annual mean air temperature (*Ta*) is ~6˚C and relative humidity (*RH*) is ~80%. Annual mean runoff at the outlet is ~700 mm (Soulsby *et al.*, 2015). Winds are commonly moderate to strong, thus, vigorous turbulence often occurs over the landscape. The majority of the catchment is covered by 0.3-0.6 m tall, dense closed-canopy heather overlying podzolic soils. Heather shrubs are evergreen with most roots in the upper 10 cm of the soils. *Sphagnum* spp. moss and other bryophytes form a dense understory beneath densely layered woody stem and branch networks of heather supporting the evergreen leaves. This results in very low light penetration through vegetation to the soil surface. Scots pine forest (*Pinus sylvestris*) is restricted to inaccessible steeper hillslopes and plantations near the catchment outlet, covering <10% of total catchment area. The riparian zones are covered by *Sphagnum* moss and grass (*Molinia caerulea).*

<Figure 1 here>

iButton sensors (DS1923 model, *Maxim Integrated,* USA) were attached to bamboo sticks hanging directly above the heather canopy (<5 cm from the top) (Figure 1c) to measure temperature and relative humidity (*RH*). The iButton sensors have a precision of ±0.5ºC and ±5% for temperature and *RH*, respectively. Sensors were shielded by two layers of white plastic bowls with the top layer wrapped by thick aluminum foils to avoid radiation influence while ensuring ventilation. To account for spatial variability of temperature and humidity above the heather canopy, 15 sensors were set up 2 m apart in an array of 3 by 5 in a representative plot, recording data every 30 min. In addition, air temperature (*Ta*), *RH*, net radiation (*Rn*), ground heat flux (*G*), wind speed/direction, and air pressure were collected from an automatic weather station (1.8 m above ground) 100 m away at 15-min intervals.

Data were collected during two time periods (TP) over one calendar year: 31/07 to 31/10 in 2015 (TP15), and 21/04 to 04/08 in 2016 (TP16). In addition, 22 throughfall collectors were placed under the heather canopies during 01/06-24/09 in 2015 to measure throughfall on a weekly basis (Braun *et al.*, 2016). Collectors comprised an inner measuring cylinder, an open orifice with a mesh screen (to prevent leaf/litter blockage) that funnels throughfall to the cylinder, and a bottom supporting part buried in ground.

2.2. Methods

The MEP model formulates the entropy production function to include the latent heat flux term. Maximization of the function under the constraint of energy conservation leads to a unique partition of net radiation into latent, sensible and ground heat fluxes for different surfaces (Wang and Bras, 2009, 2011). In this study, we adapted the model for transpiration (T) estimation in equations (1-3):

$$T = \frac{k_u \cdot Rnc}{\lambda\left(1 + B^{-1}(\sigma)\right)} \quad (1)$$

$$B(\sigma) = 6\left(\sqrt{1 + \frac{11}{36}\sigma} - 1\right) \quad (2)$$

$$\sigma(T_c, q_c) = \frac{\lambda^2}{c_p R_v} \frac{q_c}{T_c^{\ 2}} \tag{3}$$

Where k_u is for unit conversion, equals to 3.6×10^6 for transpiration in mm/h. *Rnc* is net radiation at the canopy [W/m^2]. λ is latent heat of vaporization [J/kg]. $B(\sigma)$ is the reciprocal of the Bowen ratio. σ characterizes the phase-change related state of the evaporating surface, as a function of temperature (T_c, in ºC) and specific humidity (q_c, in kg/kg) at the canopy surface, which in this study were the iButton measurements. c_p is the specific heat capacity of air at constant pressure [1013 J/(kgºC]. R_v is the gas constant for water vapor [461.5 J/(kgºC)]. Transpiration was calculated at hourly intervals and then summed up to daily values. Night-time transpiration was assumed zero because *T* in this environment is primarily controlled by radiation (Wang *et al.*, 2017).

Rnc was not directly measured but estimated based on Beer's law: $Rnc=Rn\cdot(1-e^{-\kappa\cdot LAI})$, where *Rn* is net radiation measured at the weather station. Beer's law has been commonly used for solar radiation allocation for canopy and soil (e.g., Ritchie, 1972; Wang *et al.*, 2014a). It has been found that the *Rn* intercepted by canopy can also be calculated using the Beer's law (Ross, 1981; Shuttleworth and Wallace, 1985; Yang *et al.*, 2013), since *Rn* during daylight hours is primarily determined by the solar radiation, and net longwave radiation is dependent on surface-air temperature difference which is small in the catchment. *LAI* (leaf area index) measured using a plant canopy analyzer LAI-2200C (*LI-COR Environmental*, USA) was 3.0 which is unrealistically high, because the optical sensor placed at the bottom of heather plants viewed not only the small leaves but also the well-developed stems and highly layered branches from bottom to top (Figure 1d, e). We therefore adopted the value of 1.7 from Calder et al., (1984) derived for a similar environment. Average *LAI* extracted from MODIS products (500m, 8-day) in 2015 was 1.9 (Myneni and Park, 2015) comparable to the value used. κ is the light extinction coefficient prescribed as 0.56, the average value for global shrublands (Zhang *et al.*, 2014). *LAI* and κ are influenced by canopy structure, leaf angle, solar angle (De Costa *et al.*, 1992). A sensitivity analysis is given in Figure S1 in Supplementary Materials, which shows that variations in *T* and *T/ET* ratio were sensitive to $\kappa \cdot LAI$ (e.g. an increase in $\kappa \cdot LAI$ by 10% will cause a 0.04 mm/d increase in *T* and 3.5% increase in *T*/*ET* ratio, respectively). However, heather is a slow growing evergreen species (Gimingham, 1960), and once mature, its canopy structure changes little. The setting of a constant *LAI* and κ for a 12 months period was therefore deemed reasonable for this site.

To estimate the total *ET* over the vegetated surface with the MEP model, we used *Ta*, *RH*, and *Rn*, *G* measured at a nearby weather station #1 (Figure 1). Comparisons of vapor pressure deficit at 3 weather stations in the catchment across a range of elevations (250-360 m.a.s.l, Figure S2 in Supplementary Materials) confirmed that there is a vapor equilibrium from the weather station #1 to an altitude ~100 m above. This indicates that the humid air is usually sufficiently mixed by winds from above the heather canopies to higher levels, ensuring the *ET* based on measurements at the weather station representative in the area. Evaporation (*E*) was calculated as the difference between *ET* and *T*. Note that this *E* is theoretically likely composed of soil evaporation, moss transpiration and interception loss.

To test the *ET* estimates from the MEP model, results were compared to those derived from more commonly used approaches. We used the FAO crop coefficient (*Kc*) method which has been used for *ET* estimation for various vegetation communities (Cammalleri *et al.*, 2013; Rosa *et al.*, 2016). *Kc* (0.70) was estimated from the MODIS 8-day *ET* product during the growing seasons of 2015 and 2016 (Mu *et al.*, 2011) in the study site pixel which is mostly covered by heather. The *Kc* value is consistent with Johnson (1991) for a similar catchment in central Scotland, and previous modeling work in the study catchment (Ala-aho *et al.*, 2017). Two methods were used to calculate the potential evapotranspiration (*pET*) using meteorological data at the weather station #1: the Penman-Monteith equation (Allen *et al.*, 1998), denoted as pET_{PM}; and the Priestley-Taylor equation (Priestley and Taylor, 1972), denoted as pET_{PT}. The Priestley-Taylor coefficient was set to the default value 1.26. Transpiration was compared to that derived from the widely applied Hydrus-1D model (Šimůnek *et al.*, 2012). Soil hydraulic parameters were obtained from inverse modeling using the soil moisture observations at three depths. Inverse results (Figure S3 in Supplementary Materials) show that water balance estimates with Hydrus reproduced the variations in soil moisture with $R^2 \geq 0.61$ and root mean square error of 0.02 cm^3/cm^3 for all three depths. This gives an independent comparison for the MEP results. More information of the Hydrus model setup, ancillary sampling and measurements can be found in the Supplementary Materials.

Lastly, the water balance between observed rainfall and the MEP-estimated *ET* was calculated, to understand the role of heather in water partitioning in terms of transpiration and rainfall interception, and potential recharge to subsurface water storage.

3. Results

3.1. Daily dynamics of hydroclimatic variables

<Figure 2 here>

The two periods shared similar characteristics of temperature and humidity. Monitoring in 2015 (TP15, 93 days) coincided with cooling down from mid-summer to autumn with a mean daily *Ta* of 10.1±2.9ºC (mean ± one standard deviation), while TP16 (106 days) was the spring warm up with a mean *Ta* of 10.6±3.6ºC (Figure 2a). *RH* was generally high during the two periods, averaging 80.7±7.0% and 76.1±8.0%, respectively. Rainfall in the two periods (167.2 and 292.2 mm) was 33% less and 30% more than the recent decadal average respectively. Net radiation (*Rn*) decreased gradually in TP15 while large variation characterized TP16 mainly due to frequent rainfall and associated clouds. Evapotranspiration was primarily restricted by energy, reflected by a strong positive linear relationship between *pET* and *Rn* ($R^2 \geq 0.87$, $p<0.001$), followed by relative humidity ($R^2 \geq 0.63$, $p<0.001$). *pET* estimated by Priestley-Taylor equation is higher than that by Penman-Monteith equation.

3.2. Evapotranspiration and its partitioning

<Figure 3 here>

Estimated *ET* and its components (Figure 3a-b) exhibited similar dynamics, and were generally higher in TP16 (spring/summer) than TP15 (summer/autumn). Variation of *ET* were consistent with radiation and *pET* in Figure 2. In total, estimated heather *T* (143.1 mm) was about 1.4 times higher than *E* (101.5 mm). The *T*/*ET* ratio during the entire study period varied from 0.55 to 0.66, with the average of 0.59±0.02 and median of 0.59, consistent in TP15 and TP16. *T/ET* ratio was generally high on rainy days when *E* was low and then became smaller on days after rain when the proportion of interception loss increased. The bands in Figure 3b demonstrate the upper and lower bounds for *E* and *T* based on standard deviation of daily *Tc* and *RH*. *E* increased on days shortly after rain, and then decreased towards zero when rain-free days were long enough. The *T*/*ET* ratio is also affected by the *LAI* and light extinction coefficient *κ* (Figure S1). The sensitivity analysis shows that when *κ·LAI* is increased by 10%, *T* increases by 0.04 mm/d and the *T/ET* ratio by 0.03; an increase of *κ·LAI* by 50% results in an increase of 0.17 mm/d in *T* and 0.14 in the *T/ET* ratio. As heather is a slow growing evergreen species and around 20 years old at the study site, an increase in the *κ·LAI* by 50% gives an extreme illustration of potential effects, as such rapid growth would be impossible. Further, when *LAI* increases with vegetation growth, the total *ET* usually also increases (Hu *et al.*, 2008). However, in this sensitivity analysis *ET* is calculated in the MEP model from hydroclimatic measurements at the weather station and therefore excludes vegetation growth effects on *ET* in the *κ·LAI* increasing scenarios.

The comparison of *ET* and *T* estimated by alternative methods showed that the MEP approach gave comparable estimations (Figure 3c-e). The crop coefficient method showed a good agreement with the MEP model for *ET* estimation when *pET* was calculated with the Penman-Monteith equation (R^2=0.92 and a slope of 0.94). Using the potential *ET* from the Priestley-Taylor equation, however, overestimated *ET* by about 21% compared to the MEP model, showing a linear regression slope of 0.79 and R^2=0.98 (p<0.001). This may indicate that the default Priestley-Taylor coefficient (1.26) is too high for this site. Regarding transpiration, the MEP model gave consistent results to the Hydrus-1D simulations, showing a linear regression slope of 0.88 (R^2=0.74, p<0.001).

3.3. Water partitioning in the low-energy, shrub-dominated humid catchment

<Table 1 here>

A summary of rainfall, *ET* and its components, and potential percolation for the two study periods is given in Table 1. Based on the observations and the MEP modelling results, there was a total of 459.4 mm rainfall over the two periods, and 53.3% was returned to the atmosphere through *ET*. It is worth mentioning that *E* in this case comprised soil evaporation (*Es*), moss transpiration (T_m) and interception loss (*Ei*). *Es* and T_m can be very small because of low light penetration to the soil surface caused by the heather structure. Therefore, majority of the 22.1% of rainfall is most likely attributable to *Ei* from both heather leaves and stems. Summer surface runoff at the site does not occur due to flat terrain, low intensity of rainfall and high infiltration capacity, consequently 46.7% of rainfall percolated to the underlying soil/groundwater.

4. Discussion

4.1. Using the MEP model for total *ET* estimation

Previous studies using the MEP model (Wang and Bras, 2011) focused on *E* and *T* estimations from bare soil and full vegetation surfaces at the plot scale. In this study, the agreement of *ET* from different methods suggests that the MEP model also has potential for estimating total *ET* over extensive homogenous vegetated surfaces. It is notable that the comparison in Figure 3c indicates that the default Priestley-Taylor coefficient α=1.26 was too high for our site; α is usually smaller in humid areas (Weiß and Menzel, 2008). To accommodate the actual *ET* estimation using the crop coefficient method, α=1.05 would be more realistic for our site (with a linear regression slope of 0.99 and R^2=0.98), which is consistent with other work in upland areas dominated by shrubs (Engstrom *et al.*, 2002).

To ensure the meteorological measurements at the weather station capture the total *ET* fluxes at this specific site, a vapor equilibrium from above the canopy to the level where *Ta*, *RH* and *Rn* were measured is required. This is similar to the practical setup of an eddy covariance tower (Baldocchi *et al.*, 2001) to account for the contribution of soil and vegetation to the total *ET* flux within a suitable footprint. By comparing the vapor pressure deficit at 3 weather stations (Figure S2) located at different elevations in the catchment, we can confirm this equilibrium in our humid environment, at least from the weather station #1 to nearly 100 m higher. In this sense, this study potentially extends the application of the MEP model from a plot scale assessment of *E* and *T* from bare soils and vegetation canopies to *ET* estimation over a spatially extensive vegetated surface. One such integrated set of meteorological measurements at an appropriate height can be more cost-effective compared to concurrent measurements at both the soil and canopy surfaces. With the increasing availability of high-resolution assimilation data of *Ta*, *q* and *Rn*, *G* (Liston and Elder, 2006), and remote sensing techniques for partitioning land surface temperature into soil surface temperature and canopy surface temperature (Yang and Shang, 2013), this may provide a step towards a feasible and efficient tool to map local to regional *ET* over more heterogeneous surfaces.

4.2. *ET* partitioning and canopy water balance

Despite the promising potential of the MEP model for total *ET* estimation, there are two major limitations in this study. Firstly, the difficulty of dividing *E* into specific components including *Ei*, *Es*, and *Tm*. Considering the high fractional vegetation cover, the dense closed heather canopy, and the high stem and branch density (MacDonald *et al.*, 1995) that effectively attenuate light penetration, *Es* and *Tm* were expected to be small. From the perspective of energy balance, under-canopy available energy was 38.6% of the total based on the Beer's law. Most of this radiation is intercepted by the layered stems and branches, and partly used to evaporate intercepted water when present; the rest was sensible heat to warm up the air. A very recent soil water isotope analysis shows that *Es* was <5% of net precipitation (Sprenger *et al.*, 2017), equivalent to 3% of gross rain. Therefore, majority of *E* (22.1% of rainfall) over the entire study period would have been *Ei*, which is lower than the average estimate (28% of rainfall) for a catchment mixed with trees and shrubs near the Scotland-England border (Robinson *et al.*, 1998).

Secondly, there is a difficulty in completely distinguishing canopy evaporation from transpiration under wet conditions, because the iButton sensed *Ta* and *RH* will likely include the influence of both T and Ei. The rainy day time (7:00-19:00) represented only 6.8% of the total day time (based on 15-min measurements). However, during such times, the site received >63% of the total rainfall. Apart from stemflow, the rest of interception would have been on the leaves and stems. The water on leaves evaporates first in a short time after rains when there is available energy, followed by transpiration. This is believed to be the main period when the effects of evaporation and transpiration on iButton sensed Tc and RH coexist. Storage on stem surfaces will evaporate with energy available below the canopy, but this process should not affect the measurements too much because of the sensors positions. This part of interception loss would have been the main source of E in addition to Es and Tm on rain-free days. Direct throughfall measurements in June-September 2015 indicated about 38% of rain was intercepted though stemflow was not measured (Braun *et al.*, 2016). The estimated Ei was 20.8% of rainfall when both Es and Tm are assumed as 3% in the similar period. The difference could be explained by stemflow along the heather (17.2%) which is higher than some desert shrubs (~9%) (Li *et al.*, 2016), but within the range for European shrubs (Llorens and Domingo, 2007).

Over the entire study period, the residual rainfall (46.7%) after ET loss percolated into the deeper soils, because surface runoff is negligible at the study plot due to the flat terrain and permeable podzolic soils (Tetzlaff *et al.*, 2007). Based on previous studies using geophysical surveys (Soulsby *et al.*, 2016) and a tracer-aided model (Birkel *et al.*, 2011), most of the excess rainfall beyond *ET* becomes storage in soils; then may later recharge groundwater (Tetzlaff *et al.*, 2007), and contribute to downslope riparian zones and streams through subsurface lateral flow (Blumstock *et al.*, 2016). The MEP-derived water balance highlights the qualitative and quantitative effects of vegetation on water partitioning and storage in heather dominated areas like the study site. This provides a benchmark for assessing the effects of land use change from management effects or projected future warmer conditions with dry summers and wet winters.

5. Conclusions

This study applied the MEP based *ET* model for the first time in a humid, low-energy headwater catchment. The model generally gave plausible estimates of total evapotranspiration and a first approximation of transpiration. The most encouraging finding of this study is that it shows the potential of the MEP model for assessing evaporation and transpiration under relatively uniform vegetation canopies, rather than the sharply contrasting (i.e. bare soil/vegetated conditions in previous applications). In the absence of measurements below the canopy it is difficult to precisely partition the evaporation into canopy evaporation and understory *ET*, though in the current study the latter is likely very small. Mixing of canopy evaporation and transpiration on wet days is also hard to separate with the measuring techniques in this study, though again in this case the effects are likely small and short in time. In total, over the study period, more than half of rainfall was returned to the atmosphere by *ET*, and the remaining percolated to recharge soil and groundwater. Around one third of rainfall was lost through heather transpiration and 22% as interception loss and understory *ET*. Heather shrublands, with extensive spatial coverage play a crucial role in water flow and storage in Northern upland. Understanding this role may assist land and water management in the future.

Acknowledgements

We would like to thank The Leverhulme Trust (project PLATO, RPG-2014-016) and the European Research Council (ERC, project GA 335910 VeWa) for funding. We also thank three anonymous reviewers for their invaluable comments that improved the manuscript substantially. Data in this study can be accessed upon request to the authors.

References

Ala-aho P, Soulsby C, Wang H, Tetzlaff D. 2017. Integrated surface-subsurface model to investigate the role of groundwater in headwater catchment runoff generation: a minimalist approach to parameterisation. *Journal of Hydrology* DOI: 10.1016/j.jhydrol.2017.02.023

Allen RG, Pereira LS, Raes D, Smith M. 1998. Crop evapotranspiration - Guidelines for computing crop water requirements - FAO Irrigation and drainage paper 56. *Irrigation and Drainage*: 1–15 DOI: 10.1016/j.eja.2010.12.001

Allen RG, Pruitt WO, Businger JA, Fritschen LJ, Jensen ME, Quinn FH. 1996. Evaporation and Transpiration. In *Hydrology Handbook*American Society of Civil Engineers: New York, NY; 125–252. DOI: 10.1061/9780784401385.ch04

Baldocchi DD, Falge E, Gu L, Olson R, Hollinger D, Running S, Anthoni P, Bernhofer C, Davis K, Evans R, et al. 2001. FLUXNET : A New Tool to Study the Temporal and Spatial Variability of Ecosystem-Scale Carbon Dioxide , Water Vapor , and Energy Flux Densities. *Bulletin of the American Meteorological Society* **82** (February): 2415–2434 DOI:

10.1175/1520-0477(2001)082<2415:FANTTS>2.3.CO;2

Birkel C, Soulsby C, Tetzlaff D. 2011. Modelling catchment-scale water storage dynamics: Reconciling dynamic storage with tracer-inferred passive storage. *Hydrological Processes* **25** (25): 3924–3936 DOI: 10.1002/hyp.8201

Blumstock M, Tetzlaff D, Dick JJ, Nuetzmann G, Soulsby C. 2016. Spatial organization of groundwater dynamics and streamflow response from different hydropedological units in a montane catchment. *Hydrological Processes* **30** (21): 3735–3753 DOI: 10.1002/hyp.10848

Bras RL. 2015. Complexity and organization in hydrology: A personal view. *Water Resources Research* **51** (8): 6532–6548 DOI: 10.1002/2015WR016958

Braun H, Tetzlaff D, Soulsby C, Weiler M. 2016. Influence of vegetation canopies on precipitation partitioning and isotope fractionation in northern upland catchments.EGU General Assembly, held 17-22 April, 2016: Vienna Austria; p.498.

Brutsaert W. 1982. *Evaporation into the atmosphere: Theory, history, and applications*. Springer Netherlands. DOI: 10.1007/978-94-017-1497-6

Calder IR. 1986. The influence of land use on water yield in upland areas of the U.K. *Journal of Hydrology* **88** (3–4): 201–211 DOI: 10.1016/0022-1694(86)90091-0

Calder IR, Hall RL, Harding RJ, Wright IR. 1984. The Use of a Wet-Surface Weighing Lysimeter System in Rainfall Interception Studies of Heather (calluna vulgaris). *Journal of Climate and Applied Meteorology* **23** (3): 461–473 DOI: Doi 10.1175/1520-0450(1984)023<0461:Tuoaws>2.0.Co;2

Cammalleri C, Ciraolo G, Minacapilli M, Rallo G. 2013. Evapotranspiration from an Olive Orchard using Remote Sensing-Based Dual Crop Coefficient Approach. *Water Resources Management* **27** (14): 4877–4895 DOI: 10.1007/s11269-013-0444-7

Caylor KK, D'Odorico P, Rodriguez-Iturbe I. 2006. On the ecohydrology of structurally heterogeneous semiarid landscapes. *Water Resources Research* **42** (7): n/a-n/a DOI: 10.1029/2005WR004683

Chen F, Manning KW, Lemone MA, Trier SB, Alfieri JG, Roberts R, Tewari M, Niyogi D, Horst TW, Oncley SP, et al. 2007. Description and evaluation of the characteristics of the NCAR high-resolution land data assimilation system. *Journal of Applied Meteorology and Climatology* **46** (6): 694–713 DOI: 10.1175/JAM2463.1

De Costa WAJM, Dennett MD, Biomass I, Index LA. 1992. Is Canopy Light Extinction Coefficient a Species - Specific Constant ? *Tropical Agricultural Research* **4**

Dunn SM, Mackay R. 1995. Spatial variation in evapotranspiration and the influence of land use on catchment hydrology. *Journal of Hydrology* **171** (1–2): 49–73 DOI: 10.1016/0022-1694(95)02733-6

Elmendorf SC, Henry GHR, Hollister RD, Björk RG, Boulanger-Lapointe N, Cooper EJ, Cornelissen JHC, Day TA, Dorrepaal E, Elumeeva TG, et al. 2012. Plot-scale evidence of tundra vegetation change and links to recent summer warming. *Nature*

Climate Change **2** (6): 453–457 DOI: 10.1038/nclimate1465

Engstrom RN, Hope AS, Stow DA, Vourlitis GL, Oechel WC. 2002. Priestley-Taylor alpha coefficient: variability and relationship to NDVI in Arctic tundra landscapes. *Journal of the American Water Resources Association* **38** (6): 1647–1659 DOI: 10.1111/j.1752-1688.2002.tb04371.x

Gimingham CH. 1960. Calluna vulgaris (L.) Hull. *Journal of Ecology* **48** (2): 455–483 DOI: 10.2307/2257528

Granier A. 1987. Evaluation of transpiration in a Douglas-fir stand by means of sap flow measurements. *Tree Physiology* **3** (0): 309–320

Haria AH, Price DJ. 2000. Evaporation from Scots pine (Pinus sylvestris) following natural re-colonisation of the Cairngorm mountains, Scotland. *Hydrology and Earth System Sciences* **4** (3): 451–461 DOI: 10.5194/hess-4-451-2000

Hu Z, Yu G, Fu Y, Sun X, Li Y, Shi P, Wang Y, Zheng Z. 2008. Effects of vegetation control on ecosystem water use efficiency within and among four grassland ecosystems in China. *Global Change Biology* **14** (7): 1609–1619 DOI: 10.1111/j.1365-2486.2008.01582.x

van Huijgevoort MHJ, Tetzlaff D, Sutanudjaja EH, Soulsby C. 2016. Using high resolution tracer data to constrain water storage, flux and age estimates in a spatially distributed rainfall-runoff model. *Hydrological Processes* **30** (25): 4761–4778 DOI: 10.1002/hyp.10902

IPCC. 2014. Summary for Policymakers. In *Climate Change 2014: Impacts, Adaptation, and Vulnerability. Part A: Global and Sectoral Aspects. Contribution of Working Group II to the Fifth Assessment Report of the Intergovernmental Panel on Climate Change*1–32. DOI: 10.1016/j.renene.2009.11.012

Johnson R. 1991. Effects of upland afforestation on water resources. The Balquhidder experiment 1981-1991. In *Report-- Institute of Hydrology*.

Kool D, Agam N, Lazarovitch N, Heitman JL, Sauer TJ, Ben-Gal A. 2014. A review of approaches for evapotranspiration partitioning. *Agricultural and Forest Meteorology* **184**: 56–70 DOI: 10.1016/j.agrformet.2013.09.003

Ladekarl UL, Rasmussen KR, Christensen S, Jensen KH, Hansen B. 2005. Groundwater recharge and evapotranspiration for two natural ecosystems covered with oak and heather. *Journal of Hydrology* **300** (1–4): 76–99 DOI: 10.1016/j.jhydrol.2004.05.003

Li L, Li X-Y, Zhang S-Y, Jiang Z-Y, Zheng X-R, Hu X, Huang Y-M. 2016. Stemflow and its controlling factors in the subshrub Artemisia ordosica during two contrasting growth stages in the Mu Us sandy land of northern China. *Hydrology Research* **47** (2): 409–418 DOI: 10.2166/nh.2015.253

Lindner M, Garcia-Gonzalo J, Kolström M, Green T, Reguera R, Maroschek M, Seidl R, Lexer MJ, Netherer S, Schopf A, et al. 2008. Impacts of Climate Change on European Forests and Options for Adaptation

Liston GE, Elder K. 2006. A Meteorological Distribution System for High-Resolution Terrestrial Modeling (MicroMet). *Journal of Hydrometeorology* **7** (2): 217–234

DOI: 10.1175/JHM486.1

Llorens P, Domingo F. 2007. Rainfall partitioning by vegetation under Mediterranean conditions. A review of studies in Europe. *Journal of Hydrology* **335** (1–2): 37–54 DOI: 10.1016/j.jhydrol.2006.10.032

Lu X, Liang LL, Wang L, Jenerette GD, McCabe MF, Grantz DA. 2017. Partitioning of evapotranspiration using a stable isotope technique in an arid and high temperature agricultural production system. *Agricultural Water Management* **179**: 103–109 DOI: 10.1016/j.agwat.2016.08.012

MacDonald AJ, Kirkpatrick AH, Hester AJ, Sydes C. 1995. Regeneration by natural layering of heather (Calluna vulgaris): frequency and characteristics in upland Britain. *Journal of Applied Ecology* **32** (1): 85–99 DOI: 10.2307/2404418

Miralles DG, De Jeu RAM, Gash JH, Holmes TRH, Dolman AJ. 2011. Magnitude and variability of land evaporation and its components at the global scale. *Hydrology and Earth System Sciences* **15** (3): 967–981 DOI: 10.5194/hess-15-967-2011

Miranda AC, Jarvis PG, Grace J. 1984. Transpiration and evaporation from heather Moorland. *Boundary-Layer Meteorology* **28** (3–4): 227–243 DOI: 10.1007/BF00121306

Mu Q, Zhao M, Running SW. 2011. Improvements to a MODIS global terrestrial evapotranspiration algorithm. *Remote Sensing of Environment* **115** (8): 1781–1800 DOI: 10.1016/j.rse.2011.02.019

Myneni R, Park YKT. 2015. MCD15A2H MODIS/Terra+Aqua Leaf Area Index/FPAR 8-day L4 Global 500m SIN Grid V006. *NASA EOSDIS Land Processes DAAC* Available at: https://doi.org/10.5067/MODIS/MCD15A2H.006

Noilhan J, Planton S. 1989. A Simple Parameterization of Land Surface Processes for Meteorological Models. *Monthly Weather Review* **117** (3): 536–549 DOI: 10.1175/1520-0493(1989)117<0536:ASPOLS>2.0.CO;2

Priestley CHB, Taylor RJ. 1972. On the Assessment of Surface Heat Flux and Evaporation Using Large-Scale Parameters. *Monthly Weather Review* **100** (2): 81–92 DOI: 10.1175/1520-0493(1972)100<0081:OTAOSH>2.3.CO;2

Ritchie JT. 1972. Model for predicting evaporation from a row crop with incomplete cover. *Water Resources Research* **8** (5): 1204–1213 DOI: 10.1029/WR008i005p01204

Robinson M, Moore RE, Nlsbet TR, Blackle JR. 1998. From moorland to forest : the Coalburn catchment experiment. (133): 24–27 Available at: http://nora.nerc.ac.uk/7372/1/IH_133.pdf [Accessed 12 June 2017]

Rosa RD, Ramos TB, Pereira LS. 2016. The dual Kc approach to assess maize and sweet sorghum transpiration and soil evaporation under saline conditions: Application of the SIMDualKc model. *Agricultural Water Management* **177**: 77–94 DOI: 10.1016/j.agwat.2016.06.028

Ross J. 1981. The radiation regime and architecture of plant stands. In *Tasks for Vegetation Sciences 3*, LIETH H (ed.).Springer Netherlands: Dordrecht; 391. DOI: 10.1007/978-94-009-8647-3

Schlesinger WH, Jasechko S. 2014. Transpiration in the global water cycle. *Agricultural and Forest Meteorology* **189–190**: 115–117 DOI: 10.1016/j.agrformet.2014.01.011

Serreze MC, Barry RG. 2011. Processes and impacts of Arctic amplification: A research synthesis. *Global and Planetary Change* **77** (1–2): 85–96 DOI: 10.1016/j.gloplacha.2011.03.004

Shuttleworth WJ, Wallace JS. 1985. Evaporation From Spare Crops - An Energy Combination Theory. *Quarterly Journal of The Royal Meteorological Society* **111** (469): 839–855 DOI: 10.1002/qj.49711146910

Shwetha HR, Kumar DN. 2015. Prediction of Land Surface Temperature Under Cloudy Conditions Using Microwave Remote Sensing and ANN. *Aquatic Procedia* **4** (Icwrcoe): 1381–1388 DOI: 10.1016/j.aqpro.2015.02.179

Šimůnek J, Genuchten M Van, Sejna M. 2012. HYDRUS: Model use, calibration, and validation. *Transactions of the ASABE* **55** (1987): 1261–1274 DOI: 10.1029/2002WR001340

Soulsby C, Birkel C, Geris J, Dick J, Tunaley C, Tetzlaff D. 2015. Stream water age distributions controlled by storage dynamics and nonlinear hydrologic connectivity: Modeling with high-resolution isotope data. *Water Resources Research* **51** (9): 7759–7776 DOI: 10.1002/2015WR017888

Soulsby C, Bradford J, Dick J, P. McNamara J, Geris J, Lessels J, Blumstock M, Tetzlaff D. 2016. Using geophysical surveys to test tracer-based storage estimates in headwater catchments. *Hydrological Processes* DOI: 10.1002/hyp.10889

Sprenger M, Tetzlaff D, Soulsby C. 2017. Stable isotopes reveal evaporation dynamics at the soil-plant-atmosphere interface of the critical zone. *Hydrology and Earth System Sciences Discussions* (February): 1–37 DOI: 10.5194/hess-2017-87

Stewart H, Hewitt CN, Bunce RGH. 2008. Assessing, mapping and quantifying the distribution of foliar biomass in Great Britain. *Biomass and Bioenergy* **32** (9): 838–856 DOI: 10.1016/j.biombioe.2007.12.015

Sutanto SJ, Wenninger J, Coenders-Gerrits AMJ, Uhlenbrook S. 2012. Partitioning of evaporation into transpiration, soil evaporation and interception: A comparison between isotope measurements and a HYDRUS-1D model. *Hydrology and Earth System Sciences* **16** (8): 2605–2616 DOI: 10.5194/hess-16-2605-2012

Tetzlaff D, Birkel C, Dick J, Geris J, Soulsby C. 2014. Storage dynamics in hydropedological units control hillslope connectivity, runoff generation, and the evolution of catchment transit time distributions. *Water resources research* **50** (2): 969–985 DOI: 10.1002/2013WR014147

Tetzlaff D, Buttle J, Carey SK, van Huijgevoort MHJ, Laudon H, McNamara JP, Mitchell CPJ, Spence C, Gabor RS, Soulsby C. 2015. A preliminary assessment of water partitioning and ecohydrological coupling in northern headwaters using stable isotopes and conceptual runoff models. *Hydrological Processes*: n/a-n/a DOI: 10.1002/hyp.10515

Tetzlaff D, Soulsby C, Waldron S, Malcolm IA, Bacon PJ, Dunn SM, Lilly A, Youngson AF. 2007. Conceptualization of runoff processes using a geographical information system and tracers in a nested mesoscale catchment. *Hydrological Processes* **21** (10): 1289–1307 DOI: 10.1002/hyp.6309

Wallace JS, Roberts JM, Roberts AM. 1982. Evaporation from heather moorland in north Yorkshire, England. *Hydrological research basins and their use in water resources planning : proceedings of the international symposium held in Berne, Switzerland September 21-23, 1982* Available at: http://agris.fao.org/agris-search/search.do?recordID=US201301444022 [Accessed 25 May 2017]

Wang H, Guan H, Deng Z, Simmons CT. 2014. Optimization of canopy conductance models from concurrent measurements of sap flow and stem water potential on Drooping Sheoak in South Australia. *Water Resources Research* **50** (7): 6154–6167 DOI: 10.1002/2013WR014818

Wang H, Tetzlaff D, Dick JJ, Soulsby C. 2017. Assessing the environmental controls on Scots pine transpiration and the implications for water partitioning in a boreal headwater catchment. *Agricultural and Forest Meteorology* **240–241**: 58–66 DOI: 10.1016/j.agrformet.2017.04.002

Wang J, Bras RL. 2009. A model of surface heat fluxes based on the theory of maximum entropy production. *Water Resources Research* **45** (11): n/a-n/a DOI: 10.1029/2009WR007900

Wang J, Bras RL. 2011. A model of evapotranspiration based on the theory of maximum entropy production. *Water Resources Research* **47** (3): n/a-n/a DOI: 10.1029/2010WR009392

Weiß M, Menzel L. 2008. A global comparison of four potential evapotranspiration equations and their relevance to stream flow modelling in semi-arid environments. *Adv. Geosci* **18**: 15–23 Available at: www.adv-geosci.net/18/15/2008/ [Accessed 29 May 2017]

Wilcox BP, Dowhower SL, Teague WR, Thurow TL. 2006. Long-Term Water Balance in a Semiarid Shrubland. *Rangeland Ecology & Management* **59** (November): 600–606 DOI: 10.2111/06-014R3.1

Yang Y, Shang S. 2013. A hybrid dual-source scheme and trapezoid framework-based evapotranspiration model (HTEM) using satellite images: Algorithm and model test. *Journal of Geophysical Research: Atmospheres* **118** (5): 2284–2300 DOI: 10.1002/jgrd.50259

Yang Y, Guan H, Hutson JL, Wang H, Ewenz C, Shang S, Simmons CT. 2013. Examination and parameterization of the root water uptake model from stem water potential and sap flow measurements. *Hydrological Processes* **27**: 2857–2863 DOI: 10.1002/hyp.9406

Yu M, Wang G, Parr D, Ahmed KF. 2014. Future changes of the terrestrial ecosystem based on a dynamic vegetation model driven with RCP8.5 climate projections from 19 GCMs. *Climatic Change* **127** (2): 257–271 DOI: 10.1007/s10584-014-1249-2

Zhang L, Hu Z, Fan J, Zhou D, Tang F. 2014. A meta-analysis of the canopy light extinction coefficient in terrestrial ecosystems. *Frontiers of Earth Science* **8** (4): 599–609 DOI: 10.1007/s11707-014-0446-7

Table 1 Daily average (± one standard deviation) of measured (rainfall) and estimated (evapotranspiration, transpiration, evaporation, and deep percolation) water balance components. Percentage of rainfall of total amount of each component over the study periods is also given below.

	Daily average (mm/d)		Percent of rainfall		
	31/07-31/10/2015	21/04-04/08/2016	31/07-31/10/2015	21/04-04/08/2016	Entire period
Rainfall	1.80±3.2	2.76±5.8			
Evapotranspiration	0.91±0.6	1.51±0.7	50.4%	54.9%	53.3%
Transpiration	0.53±0.3	0.89±0.4	29.2%	32.3%	31.2%
Evaporation	0.38±0.3	0.62±0.3	21.2%	22.6%	22.1%
Percolation	0.89±3.5	1.24±6.2	49.6%	45.1%	46.7%

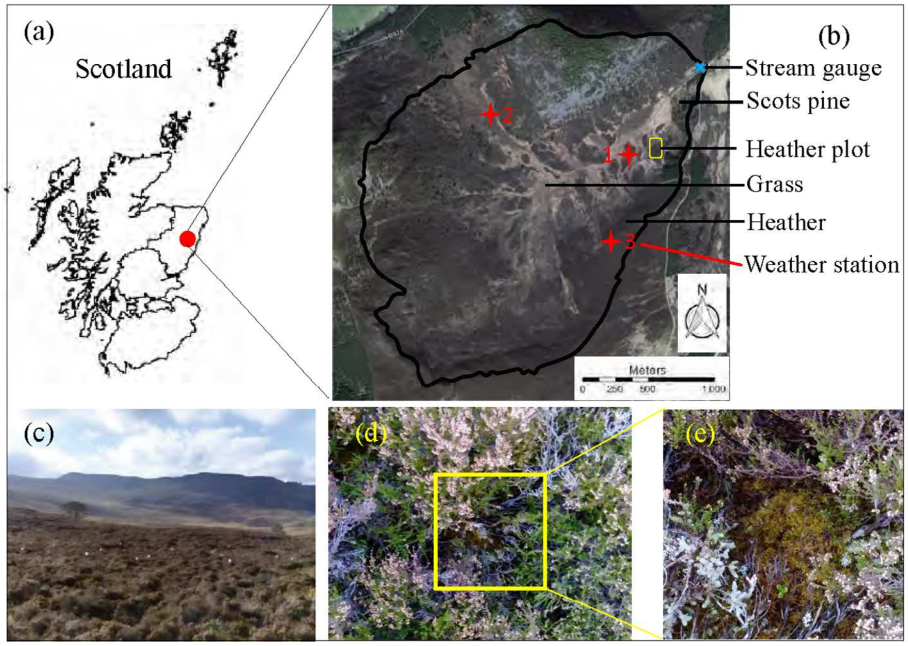

Figure 1 (a) Location of the Bruntland Burn catchment on the map of Scotland; (b) Aerial photo of the catchment showing three major vegetation types in green (Scots pine), dark brown (heather), and light brown (grass), and locations of 3 weather stations, heather plot in this study, and stream gauge at the outlet; (c) Heather plot with iButton sensors hanging right above canopies; (d) Heather canopies in December 2016; and (e) Moss cover under heather at soil surface.

254x190mm (150 x 150 DPI)

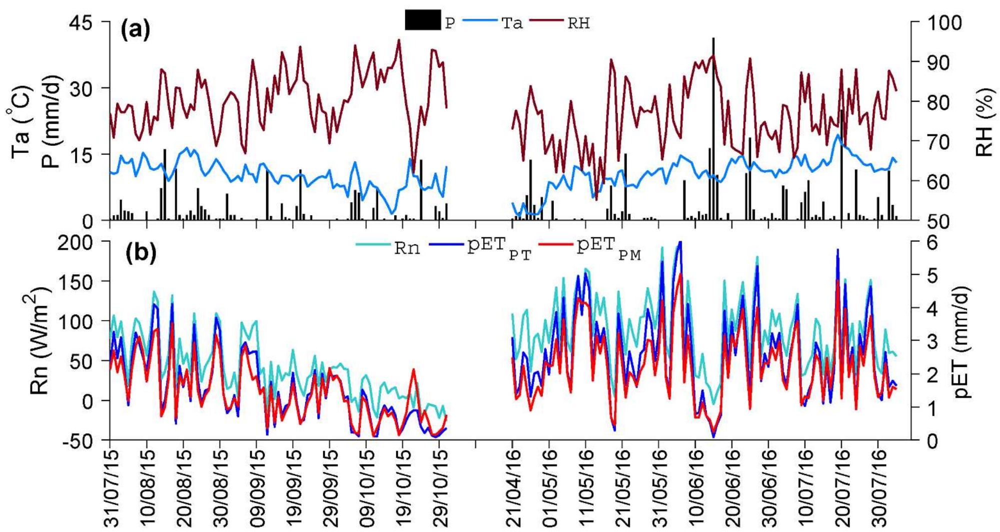

Figure 2 Daily dynamics of hydroclimatic variables at the weather station #1. (a) Air temperature (*Ta*), relative humidity (*RH*), and rainfall (*P*); (b) Net radiation (*Rn*) and potential evapotranspiration (*pET*). pET_{PT} is *pET* calculated using the Priestley-Taylor equation, and pET_{PM} is *pET* calculated using the Penman-Monteith equation. The gap separates the two measurement periods in 2015 and 2016.

227x119mm (300 x 300 DPI)

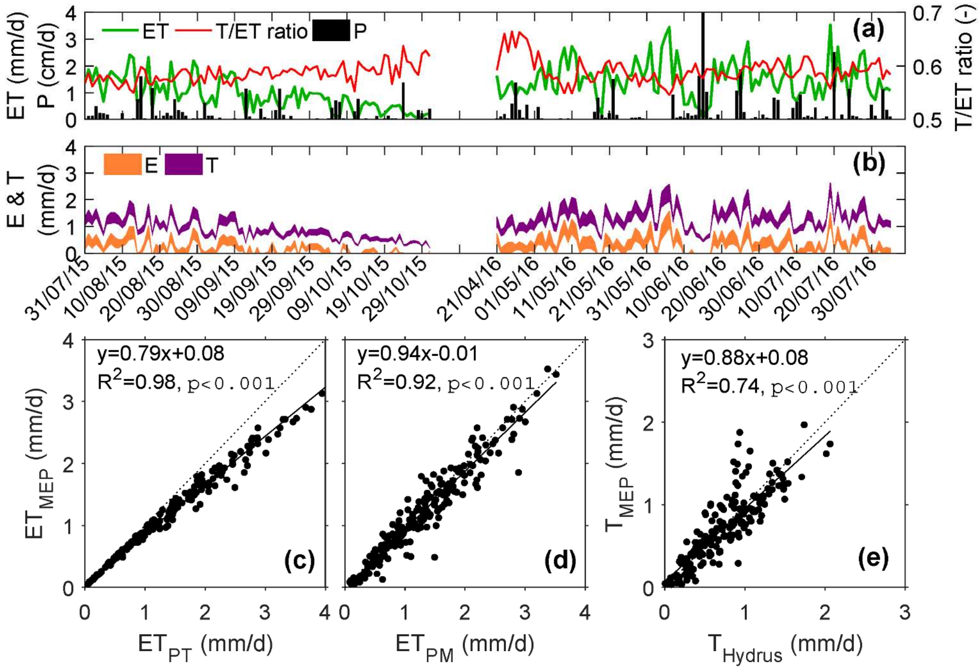

Figure 3 (a) Daily dynamics of evapotranspiration (*ET*), *T/ET* ratio and precipitation (*P*). (b) daily dynamics of evaporation (*E*) and transpiration (*T*). The bands of *E* and *T* give the upper and lower limits estimated based on daily standard deviation of temperature and humidity. The gap separates the two periods in 2015 and 2016. (c-d) Comparisons of *ET* estimated from the MEP model, FAO crop coefficient method with potential *ET* calculated by Priestley-Taylor and Penman-Monteith equations respectively. (e) Comparison of *T* by the MEP model and Hydrus-1D model. Dashed lines are 1:1 lines. Solid lines are from linear regression.

217x145mm (300 x 300 DPI)